

Application of Spectral Derivative data in spectral Near Infrared Tomography

Hamid Dehghani^a, Frederic Leblond^b, Brian W. Pogue^b and Fabien Chauchard^c

^a School of Computer Science, University of Birmingham, B15 2TT, UK

^b Thayer School of Engineering, Dartmouth College, NH 03755, USA

^c Indatech, 385 Avenues des Baronnes, Prades Le Lez, France

ABSTRACT

The use of the spectral derivative method in Near Infrared optical spectroscopy and tomographic imaging is presented, whereby instead of using discrete measurements around several wavelengths, the difference between nearest neighboring spectral measurements is used. The proposed technique is shown to be insensitive to the unknown tissue and fiber contact coupling coefficients providing substantially increased accuracy as compared to more conventional techniques. The self-calibrating nature of the spectral derivative techniques increases its robustness in clinical applications, as is demonstrated based on simulated results.

Keywords: Optical Imaging, Image reconstruction, Spectral Derivative, Tomography

1. INTRODUCTION

The use of near infrared (NIR) spectroscopy in functional imaging of soft tissue relies on the low absorption of tissue in the wavelengths range of 650 – 900 nm, and is a widely used method for the measurement of tissue function and scattering properties [1-6]. The main advantages of NIR spectroscopy and imaging is the fact that light-matter interactions in this spectral range are non-ionizing and that data acquisition can be performed on relatively fast time scales. Typically measurements of NIR light propagation through soft tissue at two or more wavelengths are used to determine the spectral absorption and scattering properties of tissue and these spectroscopy techniques to date have been used for the study of brain function [6], breast cancer detection and characterization [7]. Several other studies have combined the use of multiple source and measurement NIR spectroscopy to topographically image brain activation studies [8, 9].

Many current spectroscopy and tomographic imaging systems are capable of measuring the complete spectrum of reflected and/or transmitted NIR signals following white light excitation with high bandwidth, therefore allowing the acquisition of a comprehensive spectral dataset for the determination of tissue function and structure. In several types of biological tissues the main chromophores contributing to absorption in the NIR are oxy and deoxy-hemoglobin as well as, to a lesser extent, water. Moreover the intrinsic scattering properties of tissue have been shown to be closely related with bulk tissue scatter size and density [10]. Additionally, through the use of novel spectral imaging techniques, it has been shown that by the direct incorporation of all spectral measurements simultaneously, it is possible to estimate tissue chromophore and scattering properties with improved quantitative and qualitative accuracy [11-13].

Most spectroscopic measurements rely on pre-measurement calibration routines that are needed to determine source strength and spectral characteristics as well as camera efficiency and in case of most systems, the calibration due to the optical fiber assembly and tissue contact. However, it is well accepted that fiber and tissue contact varies from case to case and it may not be possible to allow for complete data calibration to allow accurate spectral measurement and quantification.

The use of second differential NIR spectroscopy of water to determine the mean optical path length of the neonatal brain has been previously demonstrated to monitor the absolute cerebral concentration of deoxy-hemoglobin [14]. Second-derivative preprocessing of data has also been utilized to remove spectral baselines and dc offsets [15]. Second derivative analysis of visible data (500-650 nm) have been shown to accentuate the differences between myoglobin and hemoglobin spectra and to remove baseline offsets between spectra, and decrease the effect of scattering on the spectra [16]. However, in the presence of noise in data, the use of second derivative multi-spectral data can lead to over amplification of noise in the absolute evaluation of tissue function and physiology.

In a previous small animal NIR tomography study, the use of spectral derivative data has been introduced [17]. It was demonstrated that instead of using NIR measurements at each wavelength, when the difference between each neighboring wavelength is instead utilized, the resulting reconstructed images were insensitive to source and detector coupling and location. In a recent paper the theory and concept of spectral derivative method, as applicable to NIR spectroscopy was introduced [18]. The underlying theory as to the self-calibrating nature of this technique was presented, together with the algorithm adapted for bulk parameter recovery. Detailed simulated studies were also presented whereby the effect of noise on the data was illustrated, together with preliminary experimental data demonstrating the effectiveness of the proposed method. In the study, the spectral derivative method is extended for full tomographic image reconstruction and it will demonstrated that the proposed novel technique can not only eliminate image artifacts due to known tissue/fiber contact, but can also provide better imaging metrics in terms of recovered parameter contrast and cross-talk.

2. THEORY

Assuming that scattering events dominates absorption, the light transport in tissue can be modeled using the Diffusion Approximation, which in frequency domain is given as:

$$-\nabla \cdot D\nabla\Phi(\mathbf{r},\omega) + \left(\mu_a + \frac{i\omega}{c}\right)\Phi(\mathbf{r},\omega) = S_0(\mathbf{r},\omega) \quad (1)$$

where ω is the intensity-modulation frequency of the light signal at spatial point r . μ_a is the absorption coefficient and D is the diffusion coefficient, given as $D = 1/3(\mu_a + \mu_s')$ where μ_s' is the reduced scattering coefficient. This is solved in discrete form using the finite element method (FEM) using the open source package NIRFAST[19, 20]. The fluence is a complex field (i.e. it has both a real and imaginary component), which is in turn mapped to amplitude and phase.

The best description of the air-tissue boundary is derived with an index-mismatched Robin-type condition, where the fluence at the edge of the tissue exits and does not return. Thus the flux leaving the boundary is equal to the fluence rate at the boundary, times a factor which accounts for the internal reflection of light back into the tissue, which is given as:

$$\Phi(\mathbf{r},\omega) = 2An.D\nabla\Phi(\mathbf{r},\omega) \quad (2)$$

The value of A depends upon the relative refractive index mismatch between tissue and air.

2.1 Spectral derivative data

Consider a set of reflectance or transmission spectroscopic point measurements (Y_{ij} , for $i = 1, \dots, n$ where n is the total number of detectors and $j = 1, \dots, L$ where L is the total number of wavelengths) due to a point source. The optical parameters within the volume of interest are given by absorption (μ_a) and reduced scattering coefficients (μ_s'). The tissue optical properties (absorption and reduced scatter) are a function of the wavelength of the applied source (λ), whose attenuation response depends on the concentration of each chromophore as well as on the scattering properties [21]. Assuming the main absorbers to be oxy hemoglobin (HbO), deoxy-hemoglobin (Hb) and water, Beer's law can be used to compute overall tissue absorption with reasonable accuracy,

$$\mu_a(\lambda) = \sum_{k=1}^3 \varepsilon_k(\lambda)c_k \quad (3)$$

where ε_k and c_k are the molar absorption spectra and the concentration of the k^{th} chromophore, respectively. The reduced scattering coefficient can be approximated using Mie theory

$$\mu_s' = a\lambda^{-b} \quad (4)$$

where a is assumed to be the scattering amplitude and b the scattering power. The reflectance measurements at each detector location Y_{ij} is then given by a light propagation model

$$Y_{i,j} = F(c_k, a, b, \lambda_j, s, d) \quad (5)$$

where s and d are for a given source / detector pair. The model F used in this work is the FEM diffusion model in equation 1, whereby for each wavelength λ the absorption and scattering coefficients are calculated using equations 3

and 4. The measurement $Y_{i,j}$ for each source / detector location and for each wavelength is proportional to the source power and other coupling factors to the medium, which are absorbed into a multiplicative calibration factor N_S . Similarly a calibration constant N_D applies for the detector gain factors, the coupling coefficients from the medium and the varying filter attenuation factors across the multi-spectral detection domain. Therefore, the detector measurement at each point becomes,

$$Y_{i,j} = N_S N_D F(c, a, b, \lambda_j, r_i) \quad (6)$$

Typically source power and coupling coefficient N_S is constant for all detectors (but may also vary spectrally for the un-calibrated system), whereas detector gain and coupling coefficient N_D can vary by substantial amounts depending on individual detector contact with the medium as well as the detection optics setup. In an experimental setup, although N_S can be calculated to some accuracy and the data calibrated, these coefficients depend on each volume of interest and can vary substantially from case to case, as well as the intensity of the source may have a spectral dependency.

Assuming that the source and detector coupling coefficient have a small spectral dependence, that is $N_{Sj} \approx N_{Sj+1}$ and $N_{Dj} \approx N_{Dj+1}$, the spectral derivative method can be utilized to account for these unknown coefficients. Equation 6 can be modified such that

$$\frac{Y_{i,j+1}}{Y_{i,j}} = \frac{N_{Sj+1} N_{Dj+1} F(c, a, b, \lambda_{j+1}, r_i)}{N_{Sj} N_{Dj} F(c, a, b, \lambda_j, r_i)} = \frac{F(c, a, b, \lambda_{j+1}, r_i)}{F(c, a, b, \lambda_j, r_i)} \quad (7)$$

As evident by equation 7, assuming that the coupling coefficients between neighboring wavelengths are equal, by taking the ratio of each dataset for each detector with respect to its nearest wavelength, it is possible to eliminate the effect of these errors.

2.2 Inverse Model

The goal of the inverse problem is recovery of optical parameters within the imaging domain based on the measurements of light fluence at the tissue surface. This is accomplished based on a least square error optimization method allowing the formation of images in terms of the chromophore concentrations and the scattering parameters. This is done assuming light transport can be modeled as a diffusive process and that physical quantities of interest can be expressed in terms of physiologically relevant parameters through equations 3 and 4. The inverse solution is achieved by minimizing the two-norm difference between measured fluence at all wavelengths, Φ^o , and the calculated spectral data Φ^c from a given model,

$$\Psi = \left\| \Phi^c(x) - \Phi^o \right\|_2^2 \quad (8)$$

The fluence fields are $n \times L$ elements vectors, i.e., one element for each source-detector pair and wavelength values. The vector $x = [c_k \ a \ b]$ parameterizes all the unknown in problem namely the chromophore concentrations and the scattering parameter at each node in the FEM mesh. The iterative update formula for the least square method can be derived and found to be [13, 19]

$$\Delta x = (J^T J + \rho I)^{-1} J^T \Delta \Phi^{c-o} \quad (9)$$

where typically $\Delta \Phi^{c-o} = \ln(\Phi^c) - \ln(\Phi^o) = \ln(\Phi^c / \Phi^o)$, ρ is the regularization parameter and J is the Jacobian matrix comprising the sensitivity (i.e. the rate of change of natural log of fluence with respect to a small change in x , $\delta \ln \Phi / \delta x$) for each unknown parameter:

$$J = [J_a \ J_b \ J_{c_1} \ J_{c_2} \ J_{c_3}] = \begin{bmatrix} J_{a,\lambda_1} & J_{b,\lambda_1} & J_{c_1,\lambda_1} & J_{c_2,\lambda_1} & J_{c_3,\lambda_1} \\ J_{a,\lambda_2} & J_{b,\lambda_2} & J_{c_1,\lambda_2} & J_{c_2,\lambda_2} & J_{c_3,\lambda_2} \\ \vdots & \vdots & \vdots & \vdots & \vdots \\ J_{a,\lambda_j} & J_{b,\lambda_j} & J_{c_1,\lambda_j} & J_{c_2,\lambda_j} & J_{c_3,\lambda_j} \end{bmatrix} \quad (10)$$

In the spectral derivative approach, the objective function is modified from Equation 7 to:

$$\Psi = \|\Delta\Phi^{c-o}\|_2^2 = \left\| \begin{bmatrix} \Phi_{\lambda_1}^c(x) - \Phi_{\lambda_2}^c(x) \\ \Phi_{\lambda_2}^c(x) - \Phi_{\lambda_3}^c(x) \\ \vdots \\ \Phi_{\lambda_{j-1}}^c(x) - \Phi_{\lambda_j}^c(x) \end{bmatrix} - \begin{bmatrix} \Phi_{\lambda_1}^o - \Phi_{\lambda_2}^o \\ \Phi_{\lambda_2}^o - \Phi_{\lambda_3}^o \\ \vdots \\ \Phi_{\lambda_{j-1}}^o - \Phi_{\lambda_j}^o \end{bmatrix} \right\|_2^2 \quad (11)$$

Here $\Delta\Phi^{c-o}$ denotes the finite difference operator. Equation 9 can then be modified to

$$\Delta x = (\tilde{J}^T \tilde{J} + \rho I)^{-1} \tilde{J}^T \Delta\Phi^{c-o} \quad (12)$$

where

$$\tilde{J} = [\tilde{J}_a \quad \tilde{J}_b \quad \tilde{J}_{c_1} \quad \tilde{J}_{c_2} \quad \tilde{J}_{c_3}]$$

$$= \begin{bmatrix} J_{a,\lambda_1} - J_{a,\lambda_2} & J_{b,\lambda_1} - J_{b,\lambda_2} & J_{c_1,\lambda_1} - J_{c_1,\lambda_2} & J_{c_2,\lambda_1} - J_{c_2,\lambda_2} & J_{c_3,\lambda_1} - J_{c_3,\lambda_2} \\ J_{a,\lambda_2} - J_{a,\lambda_3} & J_{b,\lambda_2} - J_{b,\lambda_3} & J_{c_1,\lambda_2} - J_{c_1,\lambda_3} & J_{c_2,\lambda_2} - J_{c_2,\lambda_3} & J_{c_3,\lambda_2} - J_{c_3,\lambda_3} \\ \vdots & \vdots & \vdots & \vdots & \vdots \\ J_{a,\lambda_{j-1}} - J_{a,\lambda_j} & J_{b,\lambda_{j-1}} - J_{b,\lambda_j} & J_{c_1,\lambda_{j-1}} - J_{c_1,\lambda_j} & J_{c_2,\lambda_{j-1}} - J_{c_2,\lambda_j} & J_{c_3,\lambda_{j-1}} - J_{c_3,\lambda_j} \end{bmatrix} \quad (13)$$

and

$$\Delta\Phi^{c-o} = \ln\left(\frac{\Phi_{j-1}^c}{\Phi_{j-1}^o}\right) - \ln\left(\frac{\Phi_j^c}{\Phi_j^o}\right) = \ln\left(\frac{\Phi_{j-1}^c \times \Phi_j^o}{\Phi_{j-1}^o \times \Phi_j^c}\right) \quad (14)$$

3. METHOD AND RESULTS

In order to demonstrate the use of spectral and spectral derivative methods on tomographic reconstruction, with and without the presence of detector noise artifacts, a set of simulated results are presented. A circular 2D FEM model with a radius of 43 mm, consisting of 1785 nodes corresponding to 3418 linear triangular elements is used. The model consists of a homogeneous background properties of HbO = 0.01 mM, Hb = 0.01 mM, water = 40%, scatter amplitude = 0.5 and scatter power of 1. Boundary data (Log Amplitude) using 16 source / detector combinations (giving a total of 240 data points) were modeled in the presence of 5 anomalies (radius 10 mm), as shown in Figure 1(a) and 1% Gaussian noise was added to simulate experimental data. For image reconstruction, the regularization parameter ρ (equation 9) used was 0.01 times the maximum of the diagonal of the Hessian ($J^T J$) and was reduced at each iteration by a factor of $10^{0.25}$ and in all cases the iteration was stopped when the projection error change as compared to the previous iteration was less than 2%. Images were then reconstructed using the spectral method outlined above, using equation 9 and shown in Figure 1(b). As evident, all anomalies are reconstructed with the poorest contrast being seen for the scatter power parameter and some crosstalk between scatter amplitude and deoxy-hemoglobin.

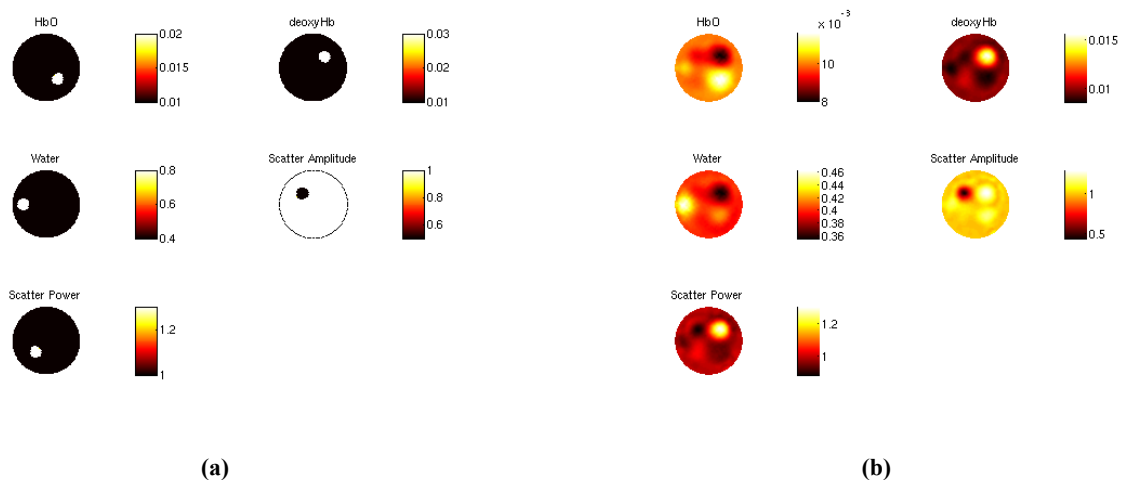


Figure 1. (a) Target model used for the generation of simulated data, and (b) Reconstructed images with 1% Gaussian noise added data using spectral technique.

Now consider the case where there exists a detector noise artifact at detector 2 (located at 4 o'clock position) and detector 9 (located at 9 o'clock position). In this example, detector 2 has a 75% efficiency and detector 9 a 41% efficiency, giving rise to a 25% and 59% attenuation in measured signal respectively. Using these detector corrupted data, together with 1% Gaussian noise, images were reconstructed using both the spectral (equation 9) and spectral derivative method (equation 12) and are shown in Figure 2. As the previous case, the regularization parameter ρ (equation 9 and 12) used was 0.01 times the maximum of the diagonal of the Hessian and was reduced at each iteration by a factor of $10^{0.25}$ and all cases iterations were stopped when the projection error change as compared to the previous iteration was less than 2%. As evident in the reconstructed images, using the spectral method (figure 2(a)), the effect of detector artifacts are dominant in all reconstructed parameters, with a lesser extent in the deoxy-hemoglobin and scatter power parameters. However, the effects on oxy-hemoglobin and water images are dramatic, specifically due to the larger artifact from detector 9. Using the spectral derivative methods (Figure 2(b)), the reconstructed images show little to no effect. Additionally, even compared to images reconstructed using the non-detector corrupted data (Figure 1(b)) the recovered contrast for all images show a great improvement, specifically for the scatter power parameter. Furthermore, the cross-talk between parameters is greatly improved, specifically for the oxy-hemoglobin, water, scatter amplitude and Scatter power.

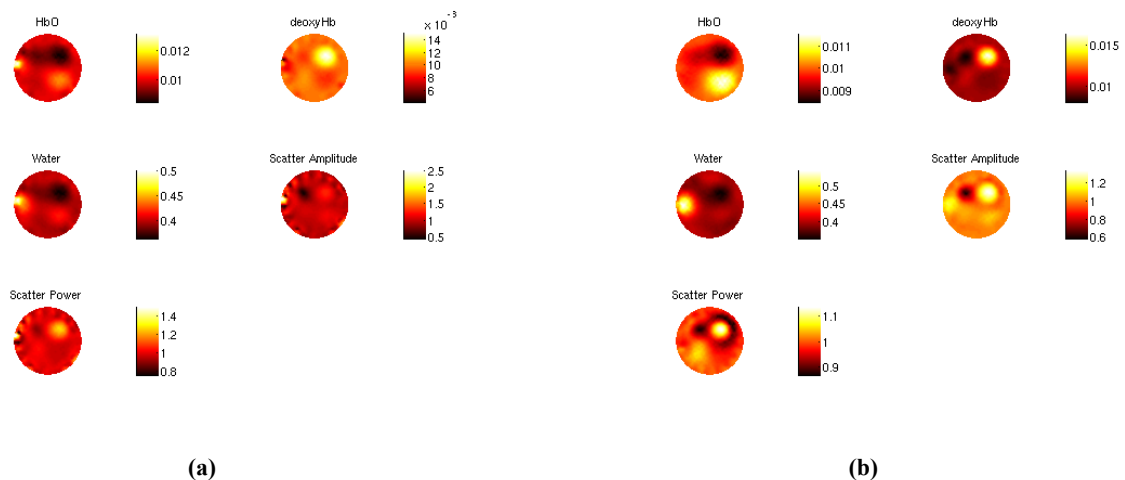


Figure 2. Reconstructed images of 'detector corrupted' data with 1% Gaussian noise added using (a) spectral technique and (b) spectral derivative technique.

4. DISCUSSIONS AND CONCLUSIONS

The concept of spectral derivative data in optical imaging is introduced, demonstrating that by the use of this technique, the effect of unknown fiber coupling with tissue can be effectively eliminated by the assumption that these coefficients have a similar value when compared with neighboring wavelengths. Using models based on the diffusion approximation, the effect of these coupling coefficients are demonstrated in tomographic image reconstruction, showing that the spectral derivative method can dramatically reduce any error. It is shown using the spectral derivative method that it is possible to calculate directly the chromophore and scattering coefficients of tissue without the need of complex, and often unreliable, data calibration routines. It is shown that using conventional spectral techniques, although the presence of small random noise in data is of little detriment, the effect of the unknown fiber coupling coefficient produced inaccurate results preventing the use of such techniques as diagnostic tools when calibration is not done correctly. Further work is planned to investigate the effect of the wavelength resolution, number of measurements and wavelength selection to improve the accuracy of the proposed method further.

ACKNOWLEDGMENTS

The work has been in part funded by the Engineering and Physical Sciences Research Council, United Kingdom, and by the National Institute of Health (NIH) Grant R01CA120368 and Award K25CA138578 from the National Cancer Institute. The author is grateful for funding from the Wellcome Trust through its Development grant which allowed collaboration between the authors possible.

REFERENCES

1. Chance, B., *Near-infrared (NIR) optical spectroscopy characterizes breast tissue hormonal and age status*. Academic Radiology, 2001. **8**(3): p. 209-10.
2. Delpy, D.T. and M. Cope, *Quantification in tissue near-infrared spectroscopy*. Phil. Trans. R. Soc. Lond. B, 1997. **352**: p. 649-659.
3. Mancini, D.M., et al., *Validation of near-infrared spectroscopy in humans*. Journal of Applied Physiology, 1994. **77**(6): p. 2740-7.
4. Tromberg, B.J., et al., *Non-invasive in vivo characterization of breast tumors using photon migration spectroscopy*. Neoplasia (New York), 2000. **2**(1-2): p. 26-40.
5. Leung, T.S., et al., *Estimating a modified Grubb's exponent in healthy human brains with near infrared spectroscopy and transcranial Doppler*. Physiological Measurement, 2009. **30**(1): p. 1-12.
6. Smith, M. and C. Elwell, *Near-Infrared Spectroscopy: Shedding Light on the Injured Brain*. Anesthesia and Analgesia, 2009. **108**(4): p. 1055-1057.
7. Shah, N., et al., *Noninvasive functional optical spectroscopy of human breast tissue*. Proceedings of the National Academy of Sciences of the United States of America, 2001. **98**(8): p. 4420-5.
8. Fantini, S., et al., *Non-invasive optical mapping of the piglet in real time*. Opt. Exp., 1999. **4**: p. 308-314.
9. Taga, G., et al., *Brain imaging in awake infants by near-infrared optical topography*. Proc Natl Acad Sci U S A, 2003. **100**(19): p. 10722-7.
10. Wang, X., et al., *Image reconstruction of effective Mie scattering parameters of breast tissue in vivo with near-infrared tomography*. J Biomed Opt, 2006. **11**(4): p. 041106.
11. Corlu, A., et al., *Diffuse optical tomography with spectral constraints and wavelength optimization*. Appl. Opt., 2005. **44**(11): p. 2082-2093.
12. Eames, M.E., Wang, J., Pogue, B. W., and Dehghani, H., *Wavelength band optimization in spectral near-infrared optical tomography improves accuracy while reducing data acquisition and computational burden*. J Biomed Opt, 2008. **13**(5): p. 054037.
13. Srinivasan, S., Pogue, B. W., Jiang, S., Dehghani, H., and Paulsen, K. D., *Spectrally Constrained Chromophore and Scattering NIR Tomography Provides Quantitative and Robust Reconstruction*. Appl. Opt., 2005. **44**(10): p. 1858-1869.
14. Cooper, C.E., et al., *The noninvasive measurement of absolute cerebral deoxyhaemoglobin concentration and mean optical pathlength in the neonatal brain by second derivative near infrared spectroscopy*. Pediat. Res., 1996. **39**: p. 32-38.

15. Arakaki, L.S.L. and D.H. Burns, *Multispectral analysis for quantitative measurements of myoglobin oxygen fractional saturation in the presence of hemoglobin interference*. Applied Spectroscopy, 1992. **46**(12): p. 1919-1928.
16. Arakaki, L.S.L., D.H. Burns, and M.J. Kushmerick, *Accurate Myoglobin Oxygen Saturation by Optical Spectroscopy Measured in Blood-Perfused Rat Muscle*. Applied Spectroscopy, 2007. **61**(9): p. 978-985.
17. Xu, H., et al., *Spectral derivative based image reconstruction provides inherent insensitivity to coupling and geometric errors*. Optics Letters, 2005. **30**(21): p. 2912-2914.
18. Dehghani, H., Leblond, F., Pogue, B. W., and Chauchard, F., *Application of spectral derivative data in visible and near-infrared spectroscopy*. phys med biol, 2010. **55**(12): p. 3381-99.
19. Dehghani, H., Eames, M. E., Yalavarthy, P. K., Davis, S. C., Srinivasan, S., Carpenter, C. M., Pogue, B. W., and Paulsen, K. D., *Near Infrared Optical Tomography using NIRFAST: Algorithms for Numerical Model and Image Reconstruction Algorithms*. Communications in Numerical Methods in Engineering, 2008.
20. NIRFAST. www.nirfast.org.
21. Prah, S., *Optical Properties of Spectra*. <http://omlc.ogi.edu/spectra/>, 2009(1 November 2009).